Chemical Engineering Science 273 (2023) 118669

Contents lists available at ScienceDirect

Chemical Engineering Science

journal homepage: www.elsevier.com/locate/ces

Droplets impact on rotating cylinders

Qingwen Dai [a,b,*], Chuchen Yue [a], Wei Huang [a], Xiaolei Wang [a]

[a] College of Mechanical and Electrical Engineering, Nanjing University of Aeronautics & Astronautics, Nanjing 210016, China
[b] Institute for Nano- and Microfluidics, Technische Universitat Darmstadt, Darmstadt 64287, Germany

HIGHLIGHTS

- Droplets impact on curved surfaces is investigated.
- Droplets bouncing on rotating and wetting cylinders is reported.
- Critical conditions of droplets bouncing and depositing is provided.
- Physical mechanism of droplets bouncing on curved surfaces is revealed.

GRAPHICAL ABSTRACT

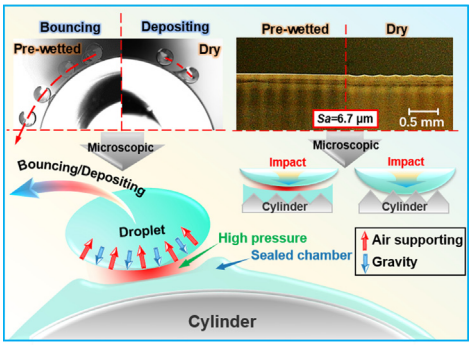

ARTICLE INFO

Article history:
Received 7 February 2023
Received in revised form 10 March 2023
Accepted 18 March 2023
Available online 23 March 2023

Keywords:
Droplet impact
Rotating cylinders
Roughness
Pre-wetting
Bouncing

ABSTRACT

In the present work, the impact dynamics of oil droplets on curved surfaces is reported. The influences of curvature, surface roughness, rotating speed, and wetting conditions on the impact dynamics are investigated. It is found that the deformation of droplets on rotating cylinders is more significant than that on static ones. An interesting bouncing phenomenon on rotating, pre-wetted, and curved surfaces is reported, and bouncing dynamics under different conditions are highlighted. Numerical simulation indicates that the sunken of liquid film on the cylinder surface generates a liquid camber there and seals compressed air, providing a cushion effect for droplets bouncing. Critical conditions are given to identify the velocity thresholds of droplets bouncing and depositing. This work provides a basic understanding of droplets impact dynamics on curved surfaces and design concepts for applications in modern industry, such as mist lubrication systems.

1. Introduction

In 1876, Worthington first reported how water droplets impact a solid plane. Since then, this fascinating phenomenon has aroused extensive attention from both academic and practice areas (Worthington, 1876). One famous proverb; water drips through a stone, manifested the continuous and powerful energy output of droplets impact responsible for erosion in nature (Sun et al., 2022). In modern industry; droplets impact has great importance for various applications including self-cleaning (Lu et al., 2015); anti-icing (Deng et al., 2012); spray cooling (Hao et al., 2015); inkjet printing (Schutzius et al., 2015; Liu et al., 2016); condensation and heat transfer (Li et al., 2016; Zhao et al., 2019); etc.

For droplet impact on flat solid surfaces, typical categories of deposition, prompt splash, corona splash, receding break-up, partial rebound, and complete rebound exist (Rioboo et al., 2001). It has been revealed that increasing impact velocity or droplet size would contribute to the deformation (Richard et al., 2002), while a higher surface tension or viscosity would restrain the deformation (Du et al., 2020). Compared to smooth surfaces, various

* Corresponding author at: College of Mechanical and Electrical Engineering, Nanjing University of Aeronautics & Astronautics, Nanjing 210016, China.
E-mail address: daiqingwen@nuaa.edu.cn (Q. Dai).

https://doi.org/10.1016/j.ces.2023.118669
0009-2509/

splashing modes occur on rough surfaces because of the rough structures (Goede et al., 2021). The bouncing phenomenon occurs once the surfaces become superhydrophobic and it can be controlled by changing the wettability (Liu et al., 2014; Chen and Li, 2010; Kolinski et al., 2014; Liu et al., 2015; Yu et al., 2021). Droplets impact and rebound on a hot plane is manifested as the famous Leidenfrost effect (Linke et al., 2006; Marin et al., 2012; Bormashenko et al., 2015).

Compared to flat surfaces, droplets impact on curved surfaces is more complex (Abolghasemibizaki et al., 2018; Sayyari et al., 2019; Taghilou and Salimi, 2019). On dry cylinders, droplets undergo the process of wetting, spreading, film drainage, and lamellae formation, and the shape of lamellas transforms with increasing curvature (Khurana et al., 2019). As impact velocity increases, droplets will rebound, spread, form an annular liquid sheet, and splash (Liang et al., 2013). Liquid films transform to a crown shape gradually with increasing surface curvature (Liang et al., 2014). For droplets impacting superhydrophobic cylinders, asymmetric rebound and stretched breakup were observed in the vertical and axial direction (Zhang et al., 2019; Liu et al., 2015). Film rebounding, breaking up, or even boiling were found on high-temperature cylinders under different Weber numbers (Guo et al., 2021).

Up to now, abundant investigations of droplets impact on flat and curved surfaces have been reported, which deeply broadens our understanding of this interfacial phenomenon and also provides different methods for droplet manipulation (Yang et al., 2017; Yang et al., 2021; Zhan et al., 2021; Dai et al., 2021; Leng et al., 2022). Actually, oil droplets impact on rotated cylinders also exists in the industry. In an aeroengine, oil droplets impact involves key processes including oil injection lubrication in the gearing box and cooling of transmission shafts (Pei et al., 2017). For oil mist lubrication systems, oil droplets impact affects the lubrication and heat transfer efficiency of transmission shafts (Zama et al., 2017). If the shaft is overheating, oil droplets bouncing is needed to cool down; while if the shaft is lacking of lubrication, oil droplets depositing is suggested. Therefore, it is vital to understand oil droplets impact on rotating cylinders. The physical properties including the viscosity and the surface tension of industrial lubricants are different from these of water droplets A review of the opening literature indicates that research on these aspects is currently lacking.

Hence, in this work, the impact dynamics of oil droplets on rotating cylinders were studied. Impact phenomena on planes and cylinders were compared, and the influence of wetting conditions and surface roughness were investigated. An interesting bouncing phenomenon on pre-wetted cylinders under specific conditions was confirmed, and critical conditions were given to identify the velocity thresholds of droplets bouncing and depositing. A numerical simulation was performed to determine the mechanism. This work provides sufficient experimental and theoretical insights into droplet impact on curved surfaces.

2. Materials and methods

2.1. Materials and test procedure

All cylinders were made of 304 stainless steel with an initial surface roughness *Sa* of 0.3 μm, and roughness surfaces were produced via different grinding processes. Different lubricants of polyalphaolefin (PAO4), olive oil, silicone oil, and paraffin oil were adopted for preliminary experiments, and the bouncing behavior of these lubricants was confirmed (Fig. S1). Considering the wide application of silicone oil in industry, and a series of selectable viscosities, silicone oils were adopted for the tests. The property of silicone oil was provided in Supplementary Table S1.

The diameter and impact velocity of droplets were controlled by the diameter and initial height of the syringe, respectively. Reynolds and Weber numbers were regulated by the impact velocity *V*, and Ohnesorge number was regulated by the viscosity μ. By placing silicone oil droplets (total volume of 20 μL) on a rotated cylinder (R_ρ = 5 mm) successively, a uniformed and slippery oil film could form on the cylinder after waiting for 2 min (Movie S1 confirms the finial wetting surface and the inset exhibits the pre-wetting process). The oil film thickness is approximately 0.06 mm (the calculation method is provided in Fig. S2).

All impact experiments were conducted at the ambient temperature of 25 °C and humidity of 40 %, the impacting process was recorded via a high-speed camera (i-SPEED 726R, iX Cameras, UK) and analyzed via image processing software.

2.2. Numerical approach

A 2D physical model (Fig. S3a) was established and a Laminar two-phase flow-phase field was adopted in numerical simulation. Navier-Stokes equation is used to calculate the velocity and pressure of single-phase flow in the laminar flow, including the mass conservation continuity equation (Eq.1), momentum conservation vector equation (Eq.2), and energy conservation equation (Eq.3) (Liu et al., 2017)

$$\frac{\partial \rho}{\partial t} + \nabla \cdot (\rho \mathbf{U}) = 0 \tag{1}$$

$$\rho \frac{\partial \mathbf{U}}{\partial t} + \rho(\mathbf{U} \cdot \nabla)\mathbf{U} = \nabla \cdot [-P\mathbf{I} + \tau] + \mathbf{F} \tag{2}$$

$$\rho C_p \left(\frac{\partial T}{\partial t} + (\mathbf{U} \cdot \nabla) T \right) = -(\nabla \cdot \mathbf{q}) + \tau : \mathbf{R} - \frac{T}{\rho} \frac{\partial \rho}{\partial T}|_p \left(\frac{\partial P}{\partial t} + (\mathbf{U} \cdot \nabla) P \right) + Q \tag{3}$$

where *P* is the pressure, and τ, and **F** are the viscous stress tensor and body force vector, respectively. In equation (3), **R** is the strain rate tensor, and its calculation formula is

$$\mathbf{R} = \frac{1}{2} \left(\nabla \mathbf{U} + (\nabla \mathbf{U})^T \right) \tag{4}$$

The phase field method is a numerical simulation technique for interface tracking and shapes modeling, which introduces the surface tension of the free liquid surface into the Navier-Stokes equations and uses a higher-order function Φ to track the gas–liquid in a two-phase flow model interface

$$\frac{\partial \Phi}{\partial t} + \mathbf{U} \cdot \nabla \Phi = \nabla \cdot \frac{\gamma \lambda}{\varepsilon^2} \nabla \psi \tag{5}$$

$$\psi = -\nabla \cdot \varepsilon^2 \nabla \Phi + \left(\Phi^2 - 1 \right) \Phi + \frac{\varepsilon^2}{\lambda} \partial f / \partial \Phi \tag{6}$$

$$\lambda = \frac{3\varepsilon\sigma}{\sqrt{8}} \tag{7}$$

where γ is the reinitialization parameter, and ε is the interface thickness control parameter. σ is the surface tension coefficient, ∂ and $f/\partial\Phi$ is the partial derivative of external free energy. When Φ = -1, the liquid behaves as the property of one phase, when Φ = 1, the liquid behaves as the property of the other phase. For the substrate, set the bottom edge as the wetted wall, and its governing equation is

$$\mathbf{U} \cdot \mathbf{n}_{wall} = 0, \mathrm{F_{fr}} = -\frac{\mu}{\beta}\mathbf{U}, \mathrm{F}_\theta = \gamma(\mathbf{n}_{\mathrm{wall}} \cdot \mathbf{n} - \cos\theta)\mathbf{n} \tag{8}$$

where F_{fr} is the friction force between solid and liquid, and β is the slip length; F_θ is introduced to control the solid–liquid contact angle. For the simulation environment, the atmospheric pressure was set to 1 atm, the temperature was set to 293.15 K, and the velocity of the droplet falling to the impact point under the effect of volume force and gravity was 0.7 m/s. For fluids, the gas used the default properties of air in COMSOL Multiphysics, the apparent contact angle of silicone oils was set to 15° in this study according to the measured value (Table S1), and the contact angle hysteresis was not considered as the impact process occurs within 0.1 s. It was assumed that there is no reaction between solid and liquid, the wall temperature was constant, the droplet was an incompressible fluid, and the fluid flow conformed to the law of laminar flow. After the 2D model was constructed, the left side was the pressure inlet (p = 0 Pa), the right side was the pressure outlet (p = 0 Pa), and the top was the open boundary (Meshes and boundary conditions for computations are provided in Fig. S3b).

Table 1
Parameter definition.

Description	Symbol
Contact angle	θ
Dynamic viscosity	μ
Radius of curvature	R_ρ
Initial diameter of a droplet	D_0
Spreading diameter of a droplet	D_s
Maximum diameter of a droplet	D_{max}
Impact velocity	V
Impact angle (angle between the impact and tangential velocity)	β
Rotational speed	ω
Maximum spreading diameter of a droplet	D_{max}
Ratio of R_ρ to D_0	$\mathcal{E}$ (R_ρ/D_0)
Tangential velocity	V_t ($\omega^* R_\rho$)
Capillary number	Ca ($\mu V/\gamma$)
Reynolds number	Re ($\rho V D_0/\mu$)
Weber number	We ($\rho V^2 D_0/\gamma$)
Ohnesorge number	Oh($We^{0.5}/Re$)
Dimensionless impact factor	P

3. Results and discussion

3.1. Droplets impact on planes and cylinders

All experimental parameters are defined in Table 1, and non-dimensional parameters of Reynolds, Weber, and Ohnesorge numbers are adopted to evaluate the impact process. Fig. 1a shows the typical impact dynamic of silicone oil droplets on the pre-wetted plane and cylinder. All droplets can bounce off these surfaces under a specific condition, and the contact time $T_{contact}$ decreases with increasing tangential velocity V_t and decreasing impact angle β (Fig. 1b). The changing trend of spreading diameter D_s divided by the initial diameter D_0 with elapsed time is shown in Fig. 1c, which increases rapidly at the initial 5 ms, and then decreases gradually. Fig. 1d shows the processes on the dry plane and cylinder (μ = 0.1 Pa·s, D_0 = 1.8 mm, R_ρ = 5 mm, and $\mathcal{E}$=3). When We = 211, droplets would spread to the maximum diameter, retract, and stabilize gradually. As We increases to 743, an obvious splash and breakup process is observed on both surfaces, and the splash film is larger on the cylinder because of the vertical spreading. Fig. 1e shows the corresponding values of D_s/D_0, which increase rapidly to a maximum value and then remains stable with elapsed time, and droplets spread wider on planes than on cylinders. For the sake of comparison, D_{max} is adopted in the following sections. Since V_t changes with R_ρ and ω, impact characteristics of oil droplets with a constant V_t (consisting of different ω and R_ρ) are provided in Fig. S4. Hereby, ω is chosen as the dominant factor of V_t in this work.

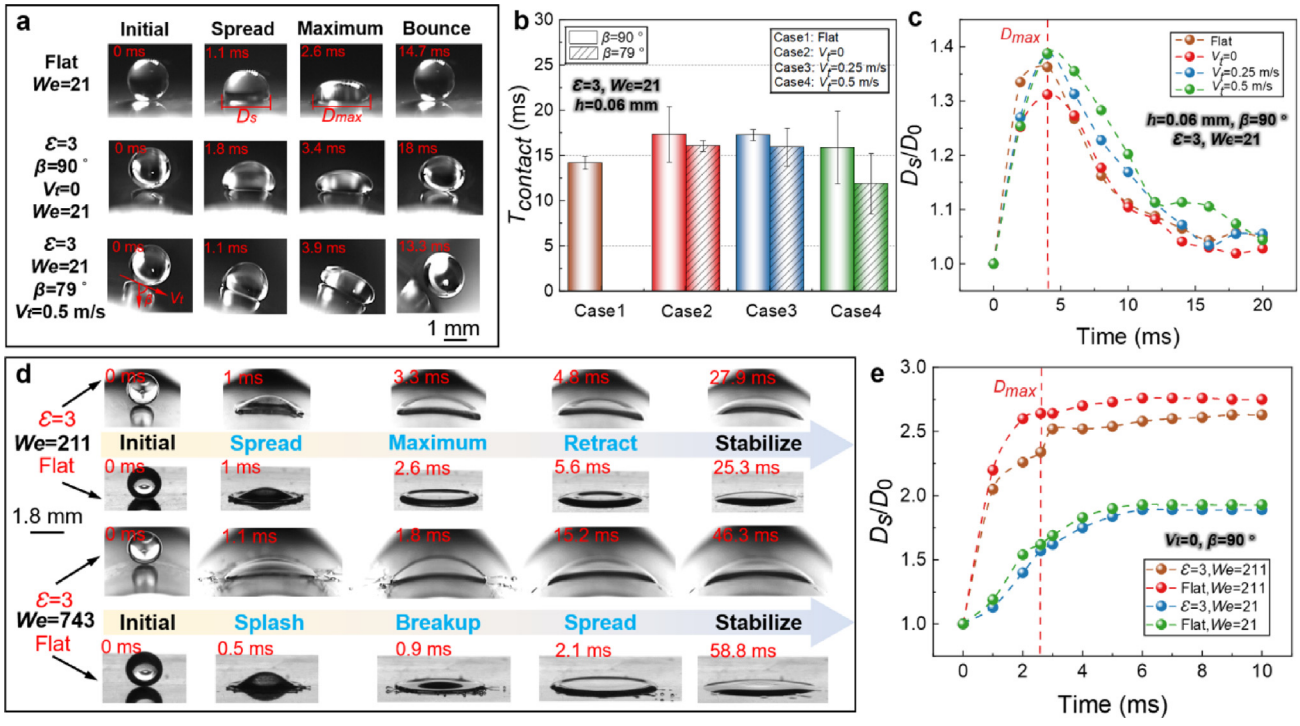

Fig. 1. Basic impact phenomena of silicone oil droplets on planes and cylinders (D_0 = 1.8 mm). Pre-wetted surfaces: (**a**) Impact dynamic under different conditions of $\mathcal{E}$= 3, We = 21, μ = 0.1 Pa·s, h = 0.06 mm, V_t = 0, 0.25, 0.5 m/s, β = 79°, 90°, and the corresponding (**b**) Contact time $T_{contact}$ and (**c**) Spreading diameter D_s/D_0. **Dry surfaces:** (**d**) Impact dynamic under different conditions of $\mathcal{E}$=3, We = 211 and 743, and the corresponding (**e**) Spreading diameter D_s/D_0.

3.2. Droplets impact on smooth and stationary cylinders

Note that the magnitude of $\mathcal{E}$ in the most existing literature ($\mathcal{E}$ < 1) (Lorenceau et al., 2004; Dressaire et al., 2016; Kim and Kim, 2016; Liu et al., 2020) is relatively lower than that in real applications. Here, $\mathcal{E}$=3 ~ 11 was investigated to quantify the impact characteristics on cylinders. Fig. 2a and b present the changing trends of D_s/D_0 with elapsed time and varying $\mathcal{E}$ under different *Re* and *We* respectively, and the impact dynamics are shown in Supplementary Movie S2. It can be seen that D_{max}/D_0 is in a positive correlation with $\mathcal{E}$, *Re,* and *We*, and this correlation becomes remarkable as *We* increase from 55 to 456 since the initial kinetic energy limits the deformation. Fig. 2c provides nonlinear expressions of D_{max}/D_0 *vs We* ($D_{max}/D_0 = 0.9*We^{0.12}$) and D_{max}/D_0 *vs Re* ($D_{max}/D_0 = 0.82*Re^{0.23}$) via data fitting. Compared to the results of Clanet *et al.* (Clanet et al., 2004), the validity of the experimental results is verified. Fig. 2d shows the changing trends of D_{max}/D_0 and T_{Dmax} (the time when D_{max} is reached) with increasing *Oh*. Note that D_{max}/D_0 is in a negative correlation with *Oh* and the maximum spread profile of droplets evolves from a concave shape at *Oh* = 0.02 to an ellipsoid shape at *Oh* = 0.83. It is accepted that inertia is the dominant resistance during initial spreading (Du et al., 2021). Since the order of magnitude of the capillary number is 1, in the case of the inertial regime, it is believed that oil droplets are in a complex force equilibrium state of inertia, capillary, and viscous forces.

3.3. Droplets impact on smooth and rotating cylinders

3.3.1. Dry surfaces

The primary difference between stationary and rotating cylinders is that a tangential force occurs once the cylinder rotates. As shown in Fig. 3a1, when $\mathcal{E}$=3, μ = 0.1 Pa·s, and V_t = 0.096 m/s, the morphology of droplet is almost undistorted at *We* = 25, and a central depression appears as *We* increases to 456. An obvious asymmetrical shape of droplets is observed as V_t increased from 0.096 to 0.288 m/s (Fig. 3a2). The asymmetrical deformation becomes more significant as *Re* increases from 20 to 95 (Fig. 3a3). It is suggested that *We* and *Re* mainly affect the spreading of droplets, and tangential velocity dominates the asymmetry. Fig. 3b shows a quantitative result of the changing trend of D_s/D_0 under the above-mentioned conditions. The cyan and red dotted lines indicate that once the droplet contacts the cylinder, it spreads rapidly due to a higher tangential force (V_t = 0.288 m/s). Increasing $\mathcal{E}$ contributes to the spreading (blue and purple dotted lines), and this enhancement can be seen in the pre-spread stage of the purple and gold dotted lines.

3.3.2. Wetted surfaces

Cylinders are always wetted in real conditions, thus, droplets impact on wetted and rotating cylinders was investigated. As shown in Fig. 3c, D_{max}/D_0 is proportional to both *Re* and V_t when droplets impact dry and pre-wetted cylinders, and D_{max}/D_0 on the

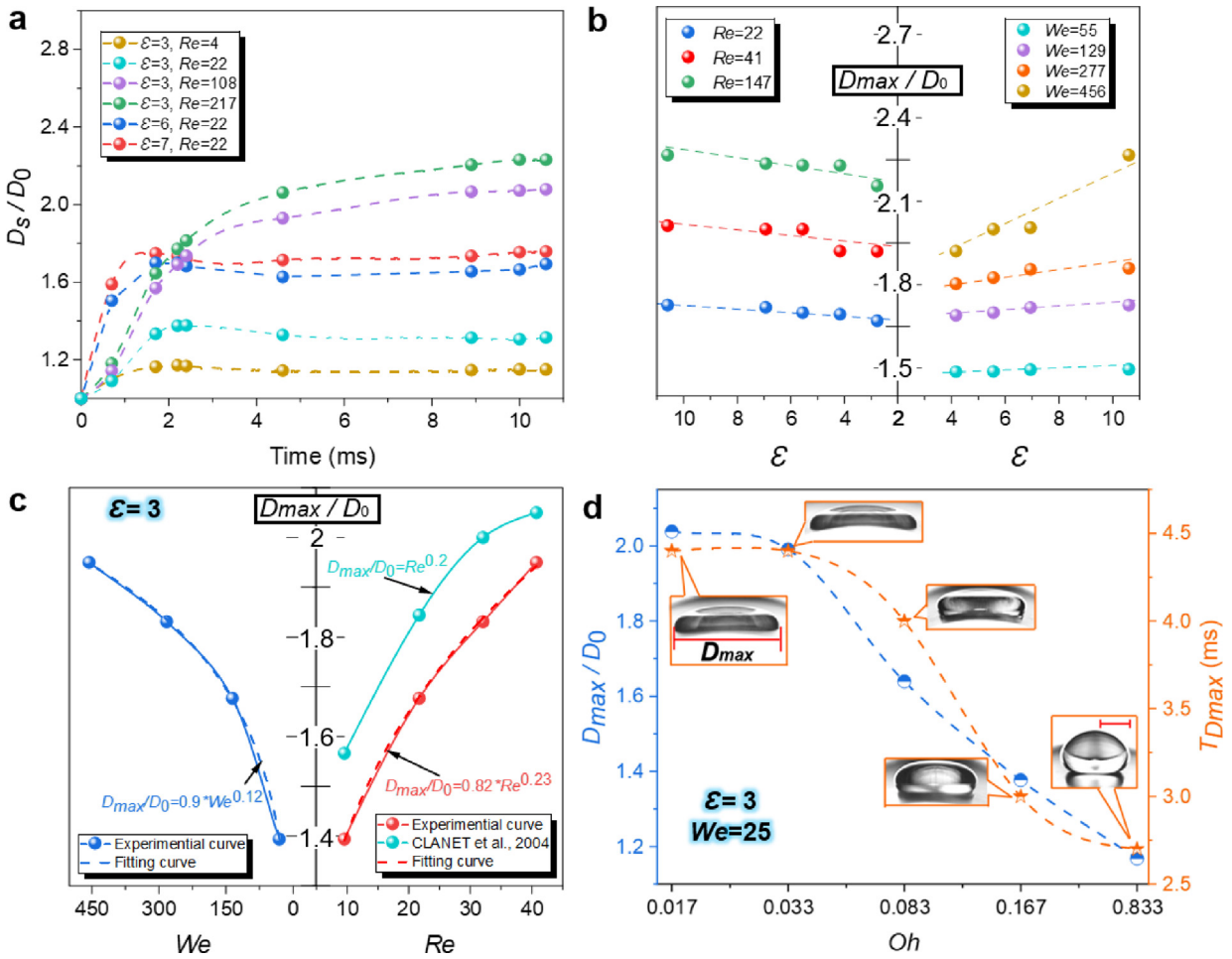

Fig. 2. Droplets impact on cylinders (D_0 = 1.8 mm). (**a**) Changing trend of D_s/D_0 with elapsed time under different $\mathcal{E}$ and *Re*. (**b**) Influence of *Re*, *We* on D_{max}/D_0 with increasing $\mathcal{E}$, (**c**) Relationship between D_{max}/D_0 and dimensionless numbers of *We* and *Re*. (**d**) Changing trends of D_{max}/D_0 and T_{Dmax} with varying *Oh*. Scale bar: 1 mm.

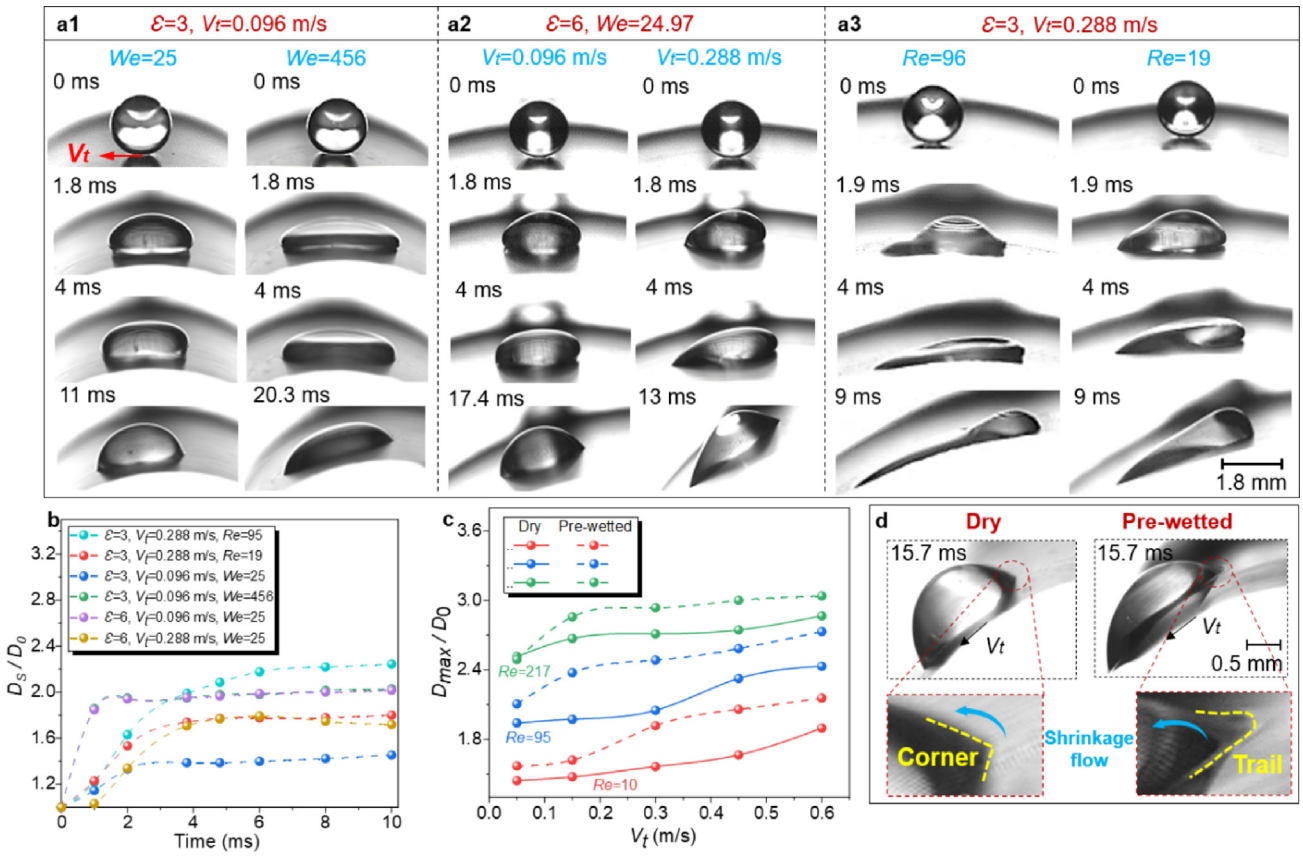

Fig. 3. Droplets impact on smooth and rotating cylinders (D_0 = 1.8 mm and counterclockwise rotation). Impact dynamics under different conditions: (**a1**) *We* of 25 and 456 at $\mathcal{E}$=3, μ = 0.1 Pa·s, and V_t = 0.096 m/s, (**a2**) V_t of 0.096 and 0.288 m/s at $\mathcal{E}$=6, μ = 0.1 Pa·s, and *We* = 25, (**a3**) *Re* of 95 and 19 at $\mathcal{E}$=3, μ = 0.1 Pa·s, and V_t = 0.288 m/s. (**b**) Changing trend of D_s/D_0 under different conditions of $\mathcal{E}$=3 and 6, V_t = 0.096 m/s and 0.288 m/s, *We* = 25 and 456, *Re* = 19 and 95. (**c**) Changing trends of D_{max}/D_0 on dry and pre-wetted cylinders under different V_t and *Re*. (**d**) Edge topography of impacted droplets on dry and pre-wetted cylinders.

pre-wetted cylinders are larger than these on dry ones, which is attributed to the merging of the edges of the droplet and the oil film on the cylinder. As the morphologies of the droplet edges on dry and pre-wetted cylinders in Fig. 3d indicate ($\mathcal{E}$=6, *We* = 25, and V_t = 0.288 m/s), the contact line is visible on the dry cylinder but doesn't exist on the pre-wetted cylinder, while the droplet tilts to the left while the right edge forms a skirt-like trail due to the shrinkage flow.

3.4. Droplets impact rough and rotating cylinders

To explore the influence of surface roughness (*Sa*) on the impact dynamic, cylinder surfaces with different *Sa* of 0.3, 1.5, 3.3, and 6.7 μm are adopted, and the micrographs are shown in Fig. 4a (more details are provided in Fig. S5). Fig. 4b shows the front and left views of droplets impact on the cylinders with *Sa* of 0.3 and 6.7 μm when *Re* = 41, $\mathcal{E}$=3, μ = 0.1 Pa·s, and V_t = 0.192 m/s. It can be seen that D_{max} on the rough cylinder (6.7 μm) is smaller than that on the smooth one(0.3 μm), and it takes 1 ms longer for the rough surface (*Sa* = 6.7 μm) to reach D_{max}.

Fig. 4c shows a quantitative result of D_{max}/D_0 on rough cylinders (*Sa*) of 0.3, 1.5, 3.3, and 6.7 μm under different conditions. When *Re* = 10, D_{max}/D_0 on these surfaces are nearly the same under a lower V_t of 0.096 m/s, and as V_t increases to 0.576 m/s, D_{max}/D_0 on the roughest surface (*Sa* = 6.7 μm) is much lower than the others. When *Re* = 41, a similar trend is confirmed that the magnitude of D_{max}/D_0 is in negative correlation with the surface roughness, and the differences become apparent with increasing V_t. It is well-known that two main wetting conditions of Wenzel and Cassie-Baxter states exist on rough surfaces (Ramachandran et al., 2015; García-Geijo et al., 2021; Jin et al., 2021). The contact angle of silicone oil on the tested surface is ~15°, Wenzel state holds, it means that menisci would form between adjacent micro asperities as the droplet spreads in the longitudinal position, and the liquid needs to full fill the gaps and overcome the Laplace pressure simultaneously (Roisman et al., 2015; Abolghasemibizaki and Mohammadi, 2017; Dai et al., 2018). It means that the rougher the surface is, the more obvious the obstruction will be. This is further verified by the measuring results of the advancing and receding contact angles on these surfaces (Fig. S6), a rougher surface has a larger advancing angle, resulting in higher resistance to spreading.

3.5. Droplets bouncing on pre-wetted cylinders

3.5.1. Bouncing phenomenon

Fig. 5a shows a typical bouncing phenomenon on the cylinder when R_ρ = 5 mm, D_0 = 1.65 mm, *V* = 0.13 m/s, and V_t = 0.5 m/s. A droplet undergoes a process of impacting, spreading to maximum, and bouncing on a wetted cylinder (Movie S3). It is interesting to see the rebound phenomenon and more experiments are performed to verify it. Fig. 5b–f shows the quantitative results of droplets impact on the pre-wetted and rotated cylinders under different conditions. It is confirmed that droplets would either bounce or deposit on the cylinders under different conditions, and there seems to be a threshold between the bouncing and depositing processes. Opening literature has proven that a dimensionless impact factor can be adopted to describe complex impact dynamics (Liang et al., 2014; Liu et al., 2022). Here, a dimensionless impact factor

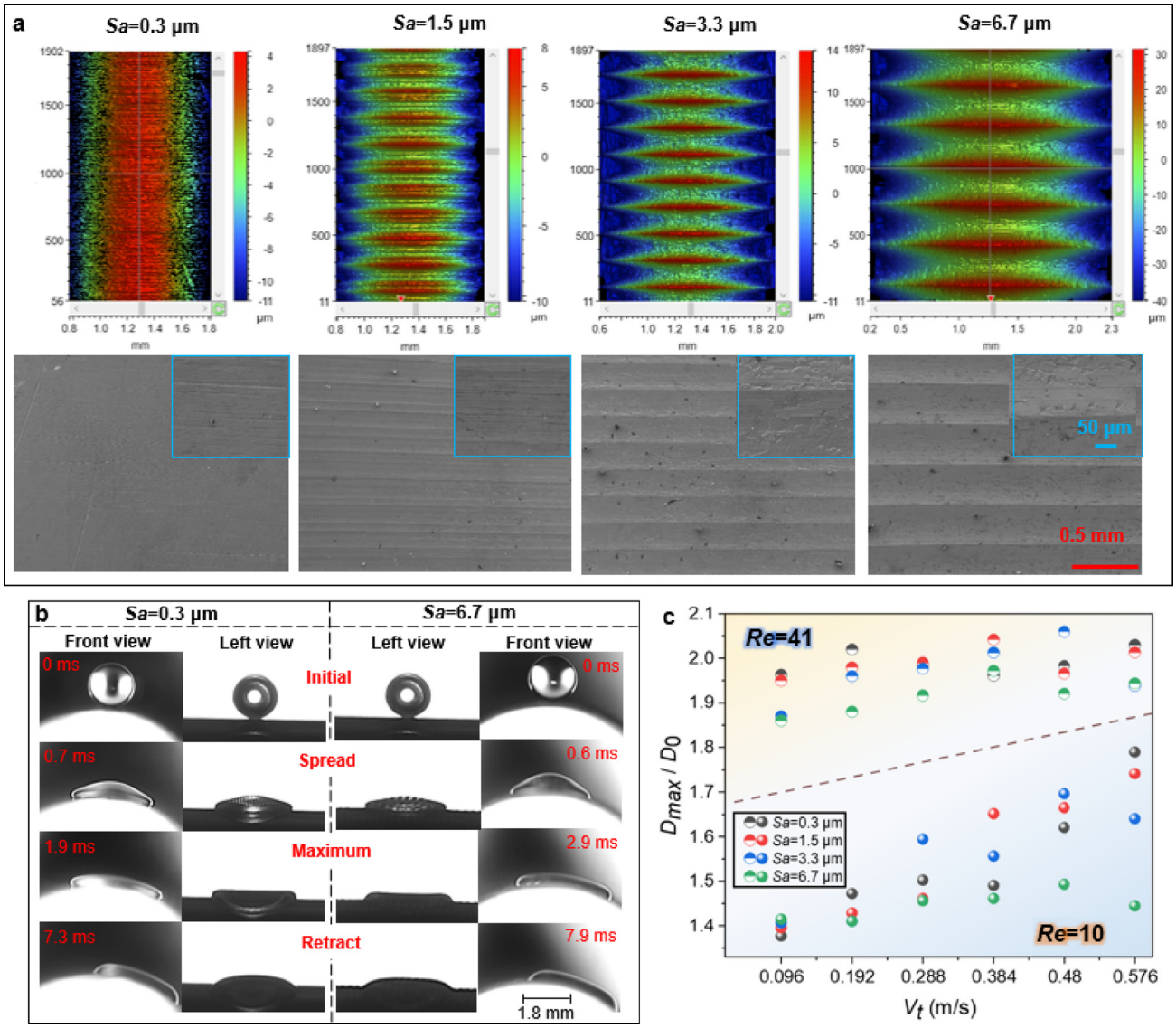

Fig. 4. Droplets impact on rotating cylinders with different roughness *Sa* (D_0 = 1.8 mm and counterclockwise rotation). (**a**) Optical and SEM microscopy of cylinders with *Sa* of 0.3, 1.5, 3.3, and 6.7 μm. (**b**) Front and left views of the impact dynamics on surfaces with *Sa* of 0.3 and 6.7 μm when *Re* = 41 and V_t = 0.192 m/s. (**c**) Effect of surface roughness on the D_{max}/D_0 under different V_t and *Re*.

(P) involving variables of V_t, V_e (unit velocity of 1 m/s), *Oh*, and β are adopted to predict the threshold of the bouncing and depositing:

$$P = \frac{(V_t + V_e)}{V_e \times Oh^{0.1}} \left(\frac{180^o - \beta}{180^o}\right)^{0.4} \quad (9)$$

Substituting all the data in Fig. 5b–f into the above formula, a general trend for the bouncing and depositing can be achieved. As shown in Fig. 5g, the upper-velocity limit (V_{Upper}) is highly responsive to the value of P, and it decreases rapidly as P increases. The lower velocity limit (V_{Lower}) is in a positive correlation with the value of P, while it increases slowly with increasing P. The upper-velocity limit (V_{Upper}) and the lower velocity limit (V_{Lower}) fit the following relationship of V_{Upper}/V_e = -0.39*P + 0.97 and V_{Lower}/V_e = 0.04*P + 0.15, respectively. Overall, these two formulas can be applied to predict the threshold of droplets bouncing and depositing on wetted cylinders.

3.5.2. Droplets bouncing at the left and the right sides

Fig. 6a shows the droplets impact process at the left (β = -79°) and the right (β = 79°) sides of a rotating cylinder. When μ = 0.0 1 Pa·s and V_t = 0.25 m/s, droplet bouncing time at the left side (20.2 ms) is much shorter than that at the right side (29.6 ms). Detailed impact processes are provided in Supplementary Movie S4. The bouncing time decreases to 26 ms as μ increases to 0.05 Pa·s due to the increased viscosity resistance (Fig. 6a3), and the droplet cannot bounce due to the high initial kinetic energy as V_t increases to 1.5 m/s (Fig. 6a4). Fig. 6b compared the D_{max}/D_0 between the left and the right sides under different conditions, it can be seen that D_{max}/D_0 is always in a positive correlation with V_t due to the pulling action of tangential motion, and in a negative correlation with μ due to the viscous resistance. When μ = 0.1 Pa·s, the range of V_t is limited because the viscous resistance obstructs droplet spreading and yields a concentrated mass distribution, resulting in depositing (no data points at high V_t). Note that the oil droplet experiences a slip before rebounding on a stationary pre-wetted

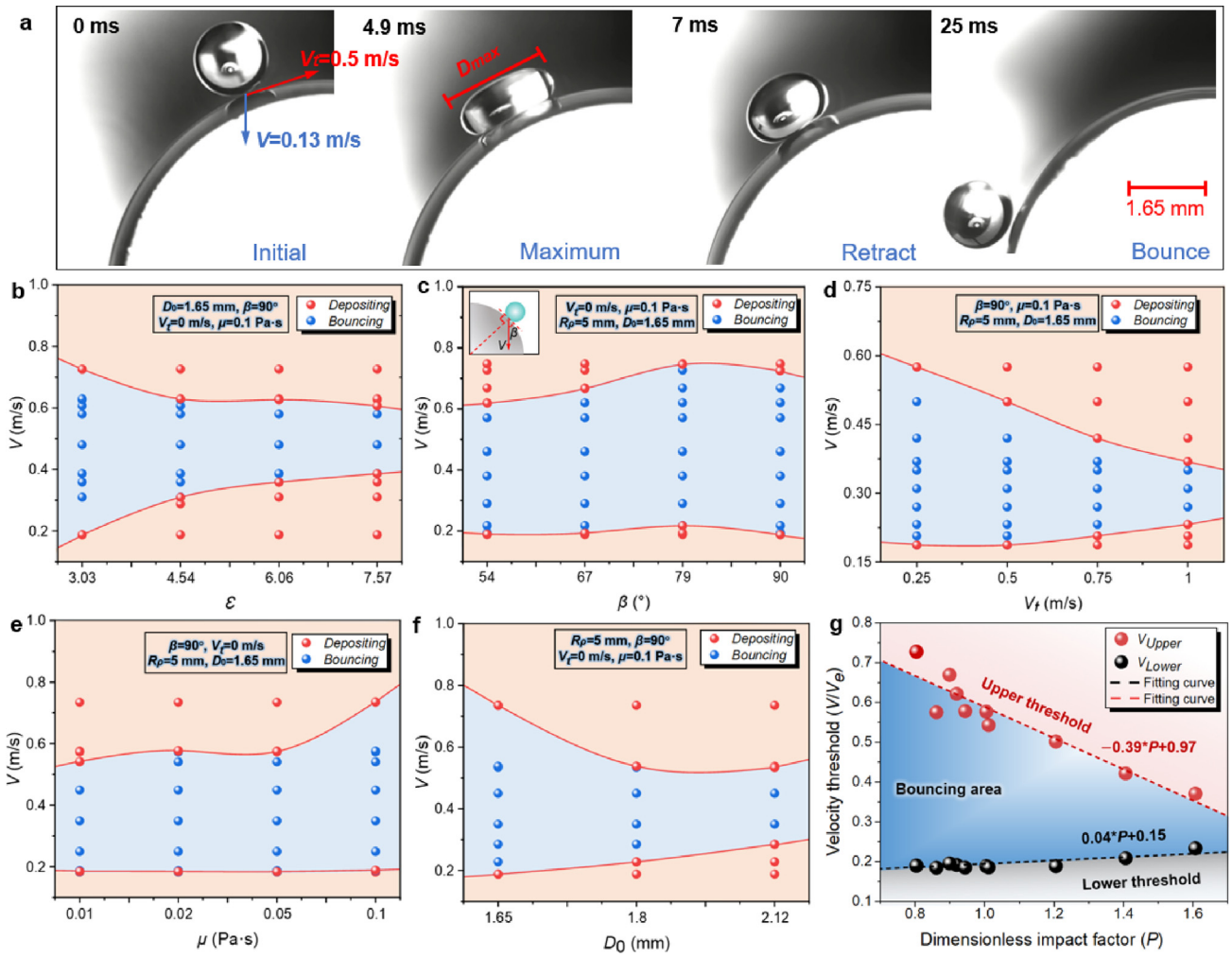

Fig. 5. Droplets bouncing on pre-wetted cylinders (clockwise rotation). (**a**) Impact dynamics on pre-wetted cylinders when R_ρ = 5 mm, D_0 = 1.65 mm, V = 0.13 m/s, and V_t = 0.5 m/s. Impact velocity threshold for droplets bouncing on cylinders under different conditions of (**b**) ε=3–8, (**c**) β = 54–90°, (**d**) V_t = 0.25–1 m/s, (**e**) μ = 0.01–0.1 Pa·s, and (**f**) D_0 = 1.65–2.12 mm. (**g**) Relationship between the velocity threshold and dimensionless impact factor (P).

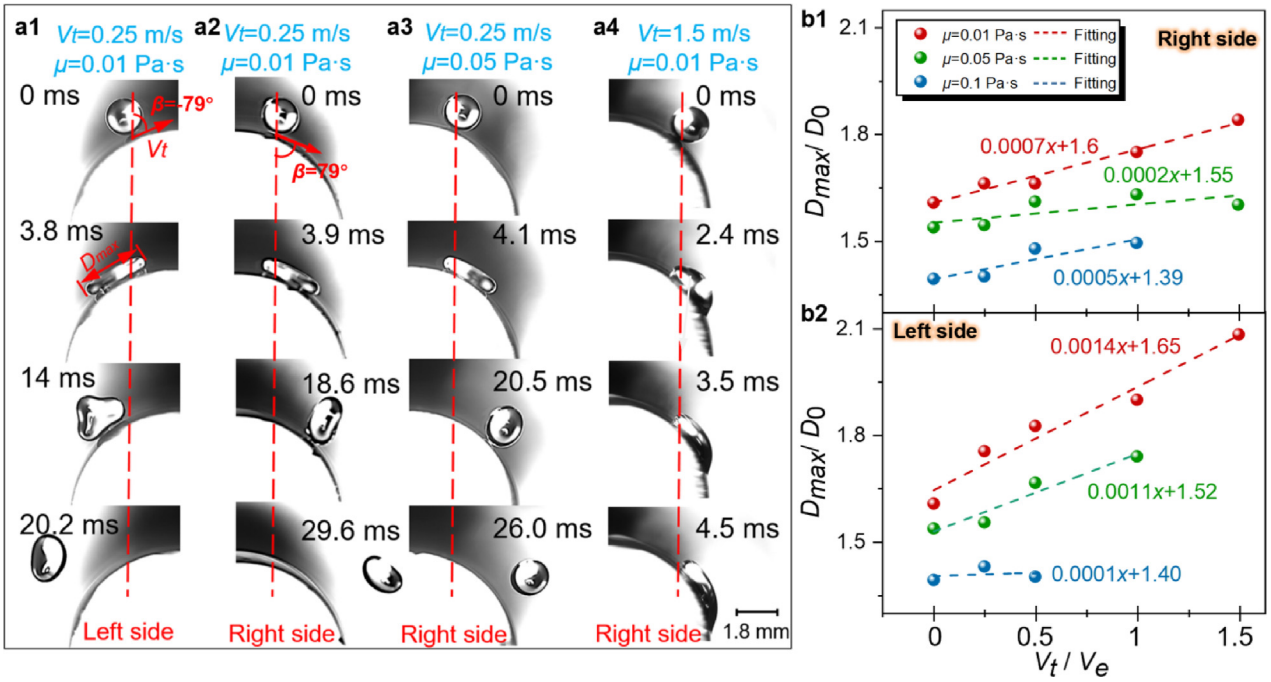

Fig. 6. Droplets bouncing at left and right sides on pre-wetted cylinders (clockwise rotation). (**a**) Detailed droplets impact processes at the left and the right sides on the pre-wetted cylinders under different V_t and μ. (**b**) Changing trend of D_{max}/D_0 with increasing ω at left and right sides.

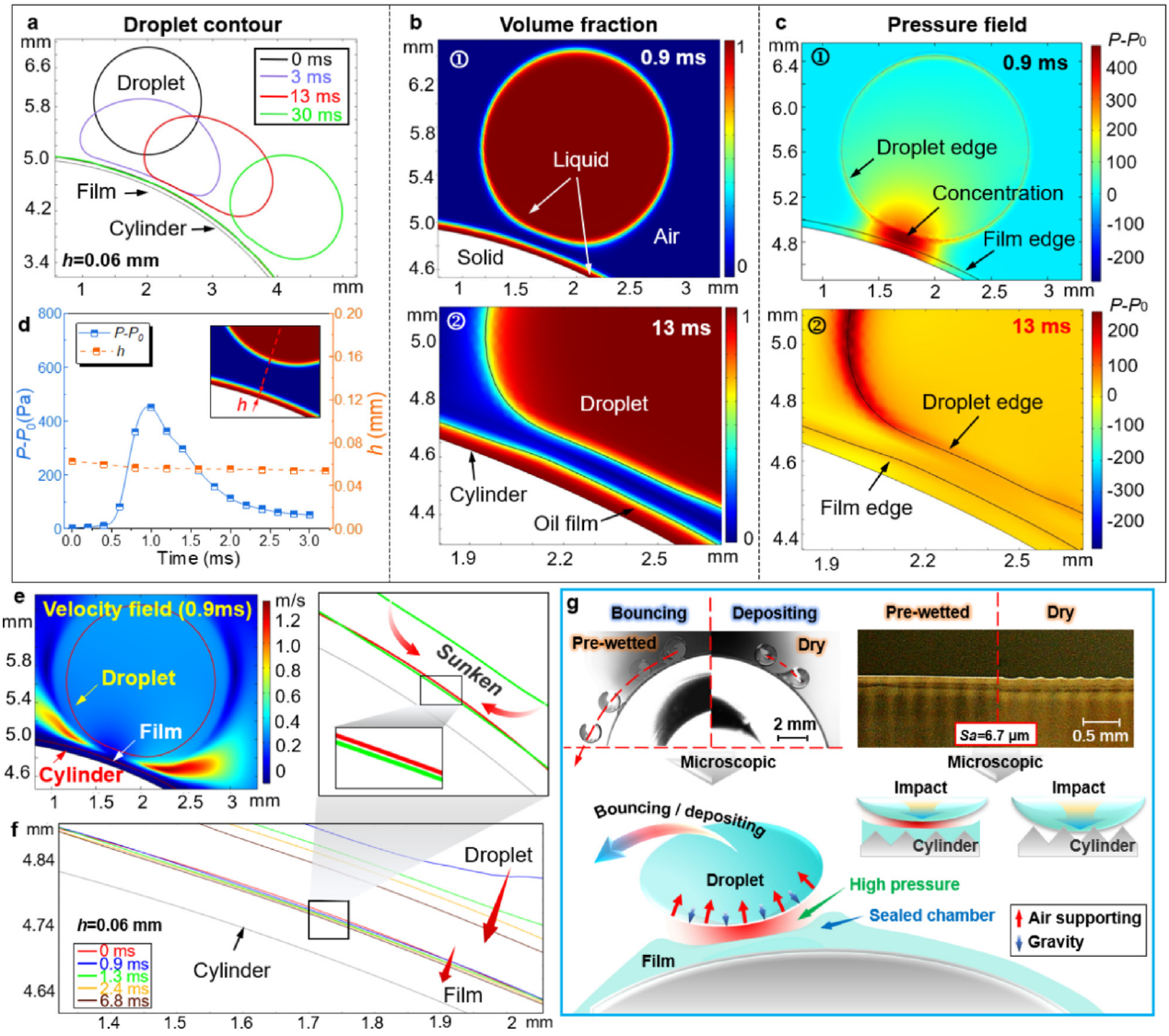

Fig. 7. Numerical simulation of a droplet impacting and bouncing on a cylinder: simulation results of (**a**) Contour line, (**b**) Volume fraction of the droplet and oil film at 0.9 and 13 ms, (**c**) Pressure field at 0.9 and 13 ms, (**d**) Changing trends of pressure difference and film thickness, (**e**) Velocity field at 0.9 ms, and (**f**) Enlarged contours of the droplet and oil film within 6.8 ms, of the droplet and the oil film under a condition of h = 0.06 mm, V = 0.7 m/s, $\mathcal{E}$=3, μ = 0.1 Pa·s, V_t = 0, β = 67°, (**g**) Schematic of the bouncing mechanism.

cylinder while not on the rotating one. It is because the droplet cannot bounce instantly on the stationary cylinder, which slips along the cylinder under the gravity within the retracting process, thus an obvious relative movement occurs (for the investigated droplets, the capillary length, $lc = \sqrt{\gamma/\rho g}$, is approximately 1.5 mm, thus gravity effect cannot be ignored). While for the rotating one, oil droplets can move downward under the action of gravity and tangential force, weakening the relative movement.

3.6. Bouncing mechanism

To figure out the underlying physical mechanism of droplets bouncing, a 2D numerical simulation was performed to model the bouncing process on a pre-wetted cylinder. Oil film with a thickness (h) of 0.06 mm was adopted for simulation under a condition of V = 0.7 m/s, $\mathcal{E}$=3, μ = 0.1 Pa·s, V_t = 0 m/s, β = 67°. Numerical results of the contour line, volume fraction, pressure field, and velocity field of the droplet and the oil film as the progress of impacting were extracted and analyzed (volume fraction and pressure field are provided in Supplementary Movie S5 and S6, respectively).

As the droplet contour indicates (Fig. 7a), a droplet undergoes a process of impacting, spreading, retracting, and bouncing off the cylinder sequentially within ~30 ms. Fig. 7b shows the volume fraction of two typical movements of initial contact and ready for bouncing. Deformation of the droplet is visible, and there is an air cushion zone between the droplet and the oil film, which contributes to the bouncing. To verify the deformation of the oil film, the pressure field in the computational domain is extracted and shown in Fig. 7c. Note that the pressure intensity between the droplet and the oil film is extremely high at the initial contact movement. The pressure concentration does not disappear immediately, which decreases with decreasing oil film thickness and recoveries to the normal pressure at ~3 ms (Fig. 7d). Referring to the volume fraction shown in Fig. 7b, it is confirmed that this pressure concentration is generated by the compressed air there. On the one hand, the pressure concentration provides an air cushion for the droplet to bounce; on the other hand, it drives the liquid film to flow on the cylinder. Furthering extracting the velocity filed at 0.9 ms and the

contour lines of oil film on the cylinder within 0–6.8 ms provides a clear insight into the origin of the formation of compressed air. As shown in Fig. 7e, the intensity of the velocity field is significantly high at both sides of the bottom of the droplet, but negligible between the bottom of the droplet and the oil film. Contour lines in Fig. 7f show the detailed deformation process of oil film, which sinks inward and forms a concave surface. The well-known Bernoulli's equation ($p + \rho v^2/2+\rho gh = Constant$, p is the pressure at the chosen point, v is the fluid flow speed at a point, h is the elevation of the point) states that an increase in the speed of a fluid occurs simultaneously with decreasing pressure, which means that a higher velocity intensity at both sides yields a lower local pressure, while a lower velocity intensity in the concave yields a higher local pressure. As a result, a sealed chamber with compressed air generates a relatively high pressure between the droplet and the oil film, providing a cushion effect for droplets bouncing. To further confirm the results, numerical simulations for oil films with two different thicknesses of h = 0.01 and 0.13 mm (compared to h = 0.06 mm, a thin and a thick oil film) are chosen and the results are presented in Fig. S7. These simulation results further support the above-mentioned mechanism.

Opening literature has revealed that when a droplet impacts a liquid pool at a low *We*, the liquid pool would be concaved and the local air would be compressed, which contributes to the bouncing of droplets (Thrivikraman et al., 2021; Maquet et al., 2016). This further corroborates the simulation presented in Fig. 7; thus, experimental results in Figs. 4–6 are understandable. The magnitude of the generated pressure concentration is in a positive correlation with the impact velocity. A lower-pressure concentration is insufficient for bouncing, and a higher-pressure concentration will drive the motion of the oil film, breaking the sealed air chamber. That is the reason why lower and upper impact velocity threshold exists in Fig. 5. A larger $\mathcal{E}$ means a flatter surface and it will diminish the camber for compressed air, a lower tangential velocity or a higher velocity would contribute to the flow of oil film, these will all enlarge the bounce areas in Fig. 5. A larger D_0 means stronger gravity, which reduces the bounce area. For the difference at the left and right sides, it is because the vector addition of the tangential velocity and the impact velocity at the left side enhances the generation of pressure concentration while weakening the pressure concentration on the right side (Fig. 6). Overall, Fig. 7g illustrates a schematic of the bouncing mechanism, in which the differences between dry and wetted cylinders are explained. It can be seen that oil can fill the micro-roughness structures on the cylinder surface, thus it is difficult for the air to escape from the interface within the impact process. As a result, a local pressure concentration is generated, and the bouncing phenomenon is observed. Therefore, droplets cannot bounce off dry and rough surfaces.

4. Conclusion

In the present work, we systematically investigated the droplet impact dynamics on rotating cylinders. The difference in droplets impact dynamic between planes and cylinders is confirmed. It is found that once the cylinders rotate, the tangential force would enhance the deformation of droplets and increase the D_{max}/D_0. Wetting the cylinder would further contribute to a high value of D_{max}/D_0 due to the merging of droplet edges and oil film. Surface roughness affects the impact process, and the rougher the surface is, the more obvious the obstruction will be. An interesting bouncing phenomenon on rotating, pre-wetted, and curved surfaces is reported. A dimensionless impact factor (P) is defined, and the critical lower velocity (V_{Lower}/V_e = 0.04*P + 0.15) and upper velocity (V_{Upper}/V_e = -0.39*P + 0.97) are given to identify the velocity threshold of droplets bouncing and depositing. Numerical simulation is carried out to figure out the underlying physical mechanism of droplets bouncing, and it is proven that the sunken of liquid film on the cylinder surface forms a liquid camber there and seals compressed air inside, yielding a cushion effect for droplets bouncing. The critical conditions of droplets bouncing and depositing on wetting and rotating cylinders provides a design concept for the modern lubrication system. One can reasonably manipulate oil droplets impact behavior by controlling these parameters to improve the efficiency of lubrication and heat transfer.

CRediT authorship contribution statement

Qingwen Dai: Conceptualization, Funding acquisition, Writing-original draft, Review & editing. **Chuchen Yue:** Investigation, Methodology, Writing-original draft, Review & editing. **Wei Huang:** Methodology, Project administration, Supervision. **Xiaolei Wang:** Methodology, Project administration, Supervision.

Data availability

Data will be made available on request.

Declaration of Competing Interest

The authors declare that they have no known competing financial interests or personal relationships that could have appeared to influence the work reported in this paper.

Acknowledgments

The authors (Q.D., C.Y., W.H., and X.W.) are grateful for the support from the National Natural Science Foundation of China (No. 51805252); Q.D. acknowledges the support from the Alexander von Humboldt Foundation; the authors would like to thank Prof. Steffen Hardt for his insightful comments and suggestion.

Appendix A. Supplementary material

Supplementary data to this article can be found online at https://doi.org/10.1016/j.ces.2023.118669.

References

Abolghasemibizaki, M., McMasters, R.L., Mohammadi, R., 2018. Towards the shortest possible contact time: Droplet impact on cylindrical superhydrophobic surfaces structured with macro-scale features. J. Colloid Interface Sci. 521, 17–23.
Abolghasemibizaki, M., Mohammadi, R., 2017. Droplet impact on superhydrophobic surfaces fully decorated with cylindrical macrotextures. J. Colloid Interface Sci. 509, 422–431.
Bormashenko, E., Bormashenko, Y., Grynyov, R., Aharoni, H., Whyman, G., Binks, B., 2015. Self-propulsion of liquid marbles: leidenfrost-like levitation driven by marangoni flow. J. Phys. Chem. C 119, 9910–9915.
Chen, L., Li, Z., 2010. Bouncing droplets on nonsuperhydrophobic surfaces. Phys. Rev. E 82, (1) 016308.
Clanet, C., BÉGuin, C., Richard, D., David, Q., 2004. Maximal deformation of an impacting drop. J. Fluid Mech. 517, 199–208.
Dai, Q.W., Huang, W., Wang, X.L., 2018. Contact angle hysteresis effect on the thermocapillary migration of liquid droplets. J. Colloid Interface Sci. 515, 32–38.
Dai, Q.W., Huang, W., Wang, X.L., Khonsari, M.M., 2021. Directional interfacial motion of liquids: Fundamentals, evaluations, and manipulation strategies. Tribol Int 154, 106749.
Deng, X., Mammen, L., Butt, H.-J., Vollmer, D., 2012. Candle soot as a template for a transparent robust superamphiphobic coating. Science 335 (6064), 67–70.
Dressaire, E., Sauret, A., Boulogne, F., Stone, H.A., 2016. Drop impact on a flexible fiber. Soft Matter 12 (1), 200–208.
Du, J., Zhang, Y., Min, Q., 2020. Numerical investigations of the spreading and retraction dynamics of viscous droplets impact on solid surfaces. Colloids Surf. A Physicochem. Eng. Asp. 125649

Du, J., Chamakos, N.T., Papathanasiou, A.G., Min, Q., 2021. Initial spreading dynamics of a liquid droplet: the effects of wettability, liquid properties, and substrate topography. Phys. Fluids 33, (4) 042118.
García-Geijo, P., Quintero, E.S., Riboux, G., Gordillo, J.M., 2021. Spreading and splashing of drops impacting rough substrates. J. Fluid Mech. 917, A50.
Goede, T.D., Bruin, K.D., Shahidzadeh, N., Bonn, D., 2021. Droplet splashing on rough surfaces. Phys. Rev. Fluid 6, (4) 043604.
Guo, C., Sun, Y., Zhao, D., 2021. Experimental study of droplet impact on superheated cylindrical surfaces. Exp. Therm. Fluid Sci. 121, 110263.
Hao, C., Li, J., Liu, Y., Zhou, X., Liu, Y., Liu, R., Che, L., Zhou, W., Sun, D., Li, L., Xu, L., Wang, Z., 2015. Superhydrophobic-like tunable droplet bouncing on slippery liquid interfaces. Nat. Commun. 6 (1), 7986.
Jin, P., Yang, J., Ren, S., Xu, H., Zhu, Y., 2021. Exploration of high precision calculation method for critical temperature of thermal reaction. Key Eng. Mater 881, 65–70.
Khurana, G., Sahoo, N., Dhar, P., 2019. Post-collision hydrodynamics of droplets on cylindrical bodies of variant convexity and wettability. Phys. Fluids 31, (2) 022008.
Kim, S.-G., Kim, W., 2016. Drop impact on a fiber. Phys. Fluids 28, (4) 042001.
Kolinski, J., Mahadevan, L., Rubinstein, S., 2014. Drops can bounce from perfectly hydrophilic surfaces. EPL 108, 24001.
Leng, X., Sun, L., Long, Y., Lu, Y., 2022. Bioinspired superwetting materials for water manipulation. Droplet 1 (2), 139–169.
Li, J., Hou, Y., Liu, Y., Hao, C., Li, M., Chaudhury, M.K., Yao, S., Wang, Z., 2016. Directional transport of high-temperature Janus droplets mediated by structural topography. Nat. Phys. 12 (6), 606–612.
Liang, G., Guo, Y., Yang, Y., Guo, S., Shen, S., 2013. Special phenomena from a single liquid drop impact on wetted cylindrical surfaces. Exp. Therm. Fluid Sci. 51, 18–27.
Liang, G., Yang, Y., Guo, Y., Zhen, N., 2014. Rebound and spreading during a drop impact on wetted cylinders. Exp. Therm. Fluid Sci. 52, 97–103.
Linke, H., Alemán, B.J., Melling, L.D., Taormina, M.J., Francis, M.J., Dow-Hygelund, C. C., Narayanan, V., Taylor, R.P., Stout, A., 2006. Self-propelled leidenfrost droplets. Phys. Rev. Lett. 96, (15) 154502.
Liu, Y., Andrew, M., Li, J., Yeomans, J.M., Wang, Z., 2015. Symmetry breaking in drop bouncing on curved surfaces. Nat. Commun. 6 (1), 10034.
Liu, J., Guo, H., Zhang, B., Qiao, S., Shao, M., Zhang, X., Feng, X.-Q., Li, Q., Song, Y., Jiang, L., Wang, J., 2016. Guided self-propelled leaping of droplets on a micro-anisotropic superhydrophobic surface. Angew. Chem. Int. Ed. 55 (13), 4265–4269.
Liu, C., Lu, C., Yuan, Z., Lv, C., Liu, Y., 2022. Steerable drops on heated concentric microgroove arrays. Nat. Commun. 13 (1), 3141.
Liu, Y., Moevius, L., Xu, X., Qian, T., Yeomans, J.M., Wang, Z., 2014. Pancake bouncing on superhydrophobic surfaces. Nat. Phys. 10 (7), 515–519.
Liu, X., Wang, K., Fang, Y., Chen, H., Shen, S., 2020. Study of the surface wettability effect on dynamic characteristics of droplet impacting a tube with different curvature ratios. Exp. Therm. Fluid Sci. 115, 110060.
Liu, Z., Wyss, H., Fernandez-Nieves, A., Shum, H.C., 2015. Dynamics of oppositely charged emulsion droplets. Phys. Fluids 27, 082003.
Liu, X., Zhao, Y., Chen, S., Zhao, X., 2017. Numerical research on the dynamic characteristics of a droplet impacting a hydrophobic tube. Phys. Fluids 29, 062105.
Lorenceau, É., Clanet, C., Quéré, D., 2004. Capturing drops with a thin fiber. J. Colloid Interface Sci. 279 (1), 192–197.
Lu, Y., Sathasivam, S., Song, J., Crick, C.R., Carmalt, C.J., Parkin, I.P., 2015. Robust self-cleaning surfaces that function when exposed to either air or oil. Science 347, 1132–1135.
Maquet, L., Sobac, B., Darbois-Texier, B., Duchesne, A., Brandenbourger, M., Dorbolo, S., Rednikov, A., Colinet, P., 2016. Leidenfrost drops on a heated liquid pool. Phys. Rev. Fluid 1, 053902.
Marin, A., Cerro, D., Römer, G., Pathiraj, B., Huis in 't Veld, A., Lohse, D., 2012. Capillary droplets on Leidenfrost micro-ratchets. Phys. Fluids 24, 122001.
Pei, Y., Qin, J., Li, X., Zhang, D., Wang, K., Liu, Y., 2017. Experimental investigation on free and impingement spray fueled with methanol, ethanol, isooctane, TRF and gasoline. Fuel 208, 174–183.
Ramachandran, R., Sobolev, K., Nosonovsky, M., 2015. Dynamics of droplet impact on hydrophobic/icephobic concrete with the potential for superhydrophobicity. Langmuir 31, 1437–1444.
Richard, D., Clanet, C., David, Q., 2002. Contact time of a bouncing drop. Nature 417 (6891), 811-811.
Rioboo, R., Marengo, M., Tropea, C., 2001. Outcomes from a drop impact on solid surfaces. At. Sprays 11, 155–166.
Roisman, I.V., Lembach, A., Tropea, C., 2015. Drop splashing induced by target roughness and porosity: the size plays no role. Adv. Colloid Interface Sci. 222, 615–621.
Sayyari, M.J., Fallah Kharmiani, S., Abolfazli Esfahani, J., 2019. A lattice Boltzmann study on dripping process during 2D droplet impact onto a wetted rotating cylinder. J. Mol. Liq 275, 409–420.
Schutzius, T.M., Jung, S., Maitra, T., Graeber, G., Köhme, M., Poulikakos, D., 2015. Spontaneous droplet trampolining on rigid superhydrophobic surfaces. Nature 527 (7576), 82–85.
Sun, T.P., Álvarez-Novoa, F., Andrade, K., Gutiérrez, P., Gordillo, L., Cheng, X., 2022. Stress distribution and surface shock wave of drop impact. Nat. Commun. 13 (1), 1703.
Taghilou, M., Salimi, A., 2019. Application of improved pseudo-potential model in examination of droplet dynamic on a rotary cylinder with high-density ratio. J. Mol. Liq 290, 111240.
Thrivikraman, N.P., Khare, A., Hegde, A.S., Harikrishnan, A.R., 2021. Confined evaporation-mediated enhanced residence time of levitated water drops over deep oil pools. Langmuir 37 (49), 14472–14482.
Worthington, A.M., 1876. On the forms assumed by drops of liquids falling vertically on a horizontal plate. Proc. R. Soc. Lond. 25, 261–272.
Yang, X.L., Song, J.L., Liu, J.K., Liu, X., Jin, Z.J., 2017. A twice electrochemical-etching method to fabricate superhydrophobic-superhydrophilic patterns for biomimetic fog harvest. Sci. Rep. 7 (1), 8816.
Yang, X.L., Zhuang, K., Lu, Y., Wang, X.L., 2021. Creation of topological ultraslippery surfaces for droplet motion control. ACS Nano 15 (2), 2589–2599.
Yu, X., Zhang, Y., Hu, R., Luo, X., 2021. Water droplet bouncing dynamics. Nano Energy 81, 105647.
Zama, Y., Odawara, Y., Furuhata, T., 2017. Experimental investigation on velocity inside a diesel spray after impingement on a wall. Fuel 203, 757–763.
Zhan, H., Lu, C., Liu, C., Wang, Z., Lv, C., Liu, Y., 2021. Horizontal motion of a superhydrophobic substrate affects the drop bouncing dynamics. Phys. Rev. Lett. 126, (23) 234503.
Zhang, H., Yi, X., Du, Y., Zhang, R., Zhang, X., He, F., Niu, F., Hao, P., 2019. Dynamic behavior of water drops impacting on cylindrical superhydrophobic surfaces. Phys. Fluids 31, (3) 032104.
Zhao, X., Zhang, B., Xi, X., Yin, Z., 2019. Analysis and prediction of single-phase and two-phase cooling characteristics of intermittent sprays. Int. J. Heat Mass Transf. 133, 619–630.